






**Pseudo-two-dimensional dynamics in a system of macroscopic rolling spheres**

M. A. López-Castaño <sup>1,\*</sup>, J. F. González-Saavedra,<sup>1</sup> A. Rodríguez-Rivas <sup>2</sup>, E. Abad <sup>3,4</sup>  
S. B. Yuste <sup>1,4</sup> and F. Vega Reyes <sup>1,4,†</sup>

<sup>1</sup>*Departamento de Física, Universidad de Extremadura, Avenida Elvas s/n, 06071 Badajoz, Spain*

<sup>2</sup>*Departamento de Matemática Aplicada II, Escuela Politécnica Superior, Universidad de Sevilla, Virgen de Africa, 7, 41011 Sevilla, Spain*

<sup>3</sup>*Departamento de Física Aplicada, Centro Universitario de Mérida, Universidad de Extremadura, 06800 Mérida, Spain*

<sup>4</sup>*Instituto de Computación Científica Avanzada (ICCAEx), Universidad de Extremadura, Avenida Elvas s/n, 06071 Badajoz, Spain*



(Received 11 December 2020; revised 17 February 2021; accepted 18 March 2021; published 16 April 2021)

We study in this work the dynamics of a collection of identical hollow spheres (ping-pong balls) that rest on a horizontal metallic grid. Fluidization is achieved by means of a turbulent air current coming from below. The upflow is adjusted so that the particles do not levitate over the grid, resulting in quasi-two-dimensional dynamics. We show that the behavior of diffusion and correlations in this system is particularly rich. Noticeably as well (and related to the complex dynamical behavior), a variety of phases appear, with important peculiarities with respect to analogous setups. We observe gas, liquid, glass, and hexagonal crystal phases. Most notably, we show that the melting of the hexagonal crystal occurs in coexistence with a liquid phase. This strikingly differs from the corresponding transition in a purely two-dimensional systems of air-fluidized disks, for which no phase coexistence has been reported in the literature.

DOI: [10.1103/PhysRevE.103.042903](https://doi.org/10.1103/PhysRevE.103.042903)

**I. INTRODUCTION**

The dynamics of macroscopic particle systems has attracted the interest of physicists and engineers since long ago [1–3]. Its significance is partly due to the potential analogies with microscopic particle systems, and partly because the manipulation of granular materials finds widespread application in industry [4]. Therefore, the understanding of what has been termed “granular dynamics” is important both from the point of view of theory and applications. More specifically, there has been an increasing interest in two-dimensional (2D) granular systems over the last decades [5,6].

Granular media share important similarities with molecular matter (as already outlined by Reynolds in 1885 [7]), but there are also significant differences and peculiarities. Convection and turbulence [8,9], jamming [10], Brownian motion [11], crystallization [5,12,13], and other phenomena well known in molecular matter have also been observed in granular matter, but they are usually more complex and they often exhibit peculiarities. Furthermore, some of the phenomenology reported in previous works is exclusive to granular matter, such as inelastic collapse [5] and clustering instabilities [14].

In particular, the attention drawn by crystallization and ordering phenomena in 2D granular systems is partly due to the impact of 2D equilibrium theories in the field of condensed matter [15,16]. The seminal work by Kosterlitz, Thouless, Halperin, Nelson, and Young [15,17,18] (subsequently extended by others [19]) highlights the role of spatial dimension, as it predicts fundamental differences in the be-

havior of two-dimensional (2D) systems with respect to that of their three-dimensional counterparts. For instance, theoretical findings and experimental observations [15,17,18] show that the crystal melting transition in 2D equilibrium systems is in general continuous and defect mediated [20]. The explanation of this 2D transition is usually referred to as the Kosterlitz-Thouless-Halperin-Nelson-Young (KTHNY) theory [19,21]. This emphasizes the interest of studying 2D granular systems. An additional advantage of such systems is that both the experimental measurements and the characterization of many properties of interest are often more straightforward than in 3D systems [22].

In order to induce granular matter thermalization, some kind of energy input is necessary, since energy is lost in macroscopic particle collisions [23]. Depending on the type of driving, experimental work in 2D systems has relied mostly on air fluidization [11,24,25] or shaking, either tangent [26] or perpendicular to the plane to which the motion is constrained. With some exceptions [27,28], in most works the plane in which the particle motion takes place coincides with the horizontal plane; hence, tangent and perpendicular shaking are equivalent to horizontal and vertical shaking, respectively. Additionally, there are some interesting shaking experiments with no gravity [29] (for which the horizontal direction is of course not defined). However, more recent work makes use of alternative methods of thermalization with the advantage that friction at the boundaries are not present, such as an AC electric field on charged particles [30] or acoustic levitators [31].

For the purpose of studying phase transitions, horizontal shaking experiments differ in that, since field gradients are generated from the boundaries, particles located near the walls will experience a net injection of energy while particles in the bulk will suffer mainly dissipative collisions, thereby

\*malopez00@unex.es

† fvega@eaphysics.xyz

giving rise to inherently inhomogeneous systems [32]; this renders the analysis of order transitions more difficult. In vertical shaking (quasi) 2D experiments, however, homogeneous dynamics can more easily be achieved. A variety of very interesting results have been obtained in vertical shaking experiments with spheres [5,6,12,13,33–37]. In particular the existence of a liquid-to-crystal continuous transition mediated by the *hexatic* phase has been confirmed, in agreement with the predictions of the KTHNY theory for equilibrium systems [21,38].

In air tables, an appropriately adjusted air current flowing from below prevents levitation of the particles (the dynamics is thus restrained to a single plane), and also generates thermal-like motion via the stochastically fluctuating turbulent wakes that are caused by the interstitial air upflow [11]. Moreover, the dynamics is found to be homogeneous if the upflow is homogeneous as well [25]. In this way, horizontal dynamics is effectively achieved (i.e., no translational kinetic energy is stored in the vertical degree of freedom) for both plane (disks [24,25]) and nonplane particles (spheres [11]).

At this stage, a comment on a subtle yet important difference between air table experiments and vertical shaking experiments [6] is in order. In the latter, there is an intrinsic (nonmeasurable) fraction of the translational kinetic energy directly input in the vertical direction via mechanical collisions between the particles and the shaking boundaries [6]. However, in air tables the motion of spheres outside the horizontal plane is limited to sphere rolling, implying that there are no vertical displacements of the center of mass of the particles. For the sake of precision, we will make use of the term *quasi-2D* or *pseudo-2D* to refer to the dynamics of rolling spheres described in this work (as already explained, for an analogous but slightly different reason, vibrated thin layers [6] are also referred to as *quasi-2D* systems) [35].

It is also important to note that, according to the type of particles in air tables, we can distinguish between works dealing with flat particles (disks, usually [24,29]), to which we will refer as two-dimensional (2D) systems and works dealing with non-plane particles, most notably, spheres [11] (as we said, we will refer to these systems as being quasi-2D). Thus, in our work, we are specifically interested in pseudo-2D dynamics, and not in strictly 2D dynamics.

As a lead-in to relevant results found throughout this work, we carried out a preliminary description of phase behavior (most notably, crystallization processes) of rolling spheres. We will see that a set of spheres on a horizontal air table may undergo a variety of different phases, ranging from the low density granular gas to highly packed crystals; unlike in quasi-2D vertical shaking experiments, where low density phases are not observable in wide regions of the parameter space [39]. Additionally, we find that repulsion forces between the spheres (of hydrodynamic origin [40]) are at play in our system, and this will have a crucial impact on the phase behavior. We have included a brief quantitative description of these phases through the computation of the appropriate bond-orientational order parameter and Voronoi diagrams. We also report results on the velocity distribution function (investigating the causes of deviations from a purely Maxwellian behavior), velocity autocorrelation, and radial distribution function; these are important to describe

the mechanisms by which particles interact with each other and to characterize the observed phases. Besides that, we have also studied the diffusive nature of our system, which is an aspect often overlooked in previous works on similar systems. An interesting takeaway is the finding of some regions (in the density-temperature parameter space) where the observed behavior is markedly subdiffusive (this being associated in some cases with a glass-like phase). We also encourage the reader to take a look at the Supplemental Material [41], where we have included a result regarding the nonmonotonic behavior of the granular temperature and some illustrative movies.

This paper is organized as follows. In the next section, we describe the experimental system and the particle tracking methods [42] we have used. In Sec. III we analyze the behavior of dynamical properties (distribution function, velocity autocorrelation and diffusion). Section IV discusses the ordering properties of the system and the emergence of phase transitions. In Sec. V we discuss the results and outline some open problems that could be studied with similar experimental setups.

## II. DESCRIPTION OF THE SYSTEM

We perform experiments with a variable number  $N$  of identical spherical particles. Specifically, our particles are ping-pong balls with diameter  $\sigma = 4$  cm (ARTENGO<sup>TM</sup> brand balls, made of ABS plastic with mass density  $0.08\text{g cm}^{-3}$ ). The spheres rest on a metallic mesh (circular holes of 3 mm diameter arranged in a triangular lattice) and are enclosed by a circular wall made of polylactic acid (PLA). The diameter of this circular boundary is  $D = 72.5$  cm and its height is  $h \simeq 4.5$  cm  $> \sigma$ . Thus, the total area of the system available to the spheres is  $A = 0.413\text{ m}^2 = 328.65 \times \pi(\sigma/2)^2$ , which means that up to  $N_{\text{max}} = (\pi/\sqrt{12}) \times 328.65 \simeq 298$  balls can fit in our system neglecting boundary effects (the  $\pi/\sqrt{12} \simeq 0.9069$  factor corresponds to the maximum packing fraction for disks in an infinite system [43]).

A state of the particulate system with stationary statistical properties is achieved by means of a vertical air flow in upward direction, as depicted in Fig. 1. This upflow through the metallic grid generated with a fan, SODECA<sup>TM</sup> HCT-71-6T-0.75/PL, and has stream velocities in the range  $u_{\text{air}} = [2-5.5]$  m/s. We have observed an approximately linear relationship between  $u_{\text{air}}$  and fan power. An intermediate foam ( $\sim 2$  cm thick) homogenizes the air current from the fan.

In order to assess the homogeneity of the flow throughout all the interstitial regions of the system, the air flow distribution over the grid was measured with a turbine digital anemometer plugged into a computer for the sake of data collection. We took measurements over a square grid of regularly spaced points on the table, and found local deviations of the air current of less than 10% with respect to the average  $u_{\text{air}}$ . The air current coming from the fan produces turbulent wakes as it flows past the spheres [44]. We thus achieve a pseudo-two-dimensional particle dynamics, since the relevant particle motion is restrained to the grid plane (for more details on our particle fluidization mediated by turbulent air flow, see the Supplemental Material [41]).

Summarizing, our experimental system has the following properties: (1) It is a many-particle system; (2) energy

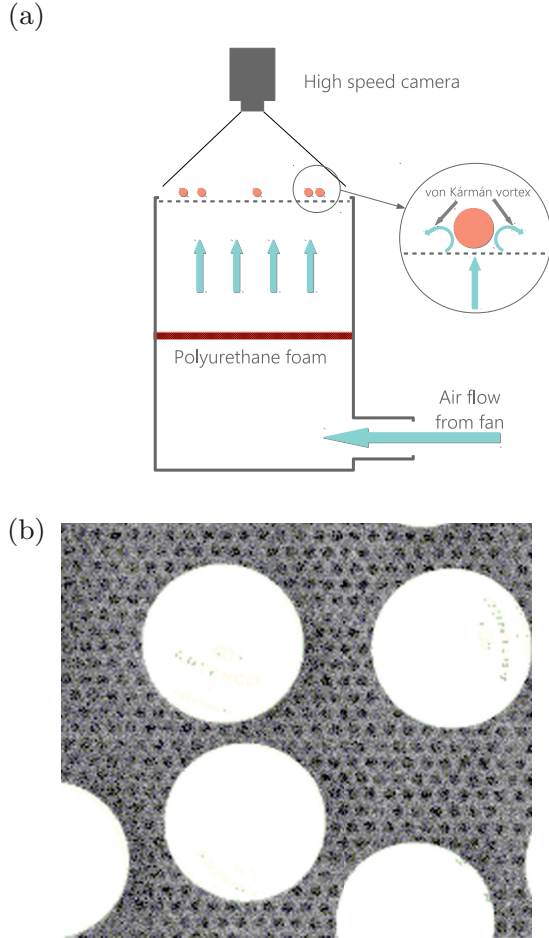


FIG. 1. (a) Sketch of the experimental setup. (b) Sample image showing the relative size of balls and grid holes.

input (in absence of particles) can be measured and is found to be homogeneous; (3) motion is contained in a horizontal plane (the grid), and as a consequence gravity does not single out a predominant direction for in-plane particle movement.

A series of experiments have been carried out by modifying the values of air flow intensity ( $2 \leq u_{\text{air}} \leq 5.5$  m/s) and packing fraction  $\phi \equiv N(\sigma/D)^2$ , ( $0.03 \leq \phi \leq 0.79$ ). We recorded a 99.92 s clip of each experiment with a high-speed camera (Phantom™ VEO 410L) at 250 frames/s, or fps, (well below the maximum operational speed of our camera); i.e., the camera records a new image every  $\Delta t_{\text{fps}} = 1/250$  s. Particle positions are detected and tracked throughout the movies by means of a particle-tracking algorithm [42,45] that, after adjusting for our particles and illumination conditions, is applied to the digital images taken by the camera. Images are recorded at the camera maximum working resolution ( $1200 \times 800$  pixels). In order to obtain high resolution images of the spheres (with 80 pixels per particle diameter), the camera was zoomed on the central region of the system; i.e., highly accurate particle position and velocity measurements were taken. More details on particle-tracking and experimental methods and as well as the measurement accuracy we achieved can be found in the Supplemental Material [41].

### III. DYNAMICAL PROPERTIES

Air-fluidized granular 2D or pseudo-2D systems have already been studied by other researchers. The closest analogs to our system may be found in the works involving air table experiments with disks (2D dynamics) [24,46–48] and with spheres (pseudo-2D dynamics) [11,40,49]. In the system with spheres, several series of experiments were initially performed with a single ping-pong ball [11] and a small number of them [40,49], in order to characterize microscopic fluctuations and particle-particle and wall-particle forces. It was only later that experiments were performed with larger sets of spheres in order to study jamming conditions [50].

Inspired by these previous works, in what follows we will extend previous studies by providing a comprehensive description of the different dynamic properties displayed by a system with a relatively large number of spheres. A full exploration of the parameter space defined by the packing fraction  $\phi$  and the granular temperature  $T$  can be achieved by controlling the number of particles  $N$  and the air upflow velocity  $u_{\text{air}}$ . We must also note that some aspects of our system dynamics differ from those of previous works for closely related systems; in particular, in our experiments particles do not appear to be trapped in a harmonic potential, as opposed to previous results [11]. Furthermore, in contrast with some previous results [24,51], we find that granular temperature does not decrease monotonically with particle density. These differences will be further discussed in the remainder of this paper.

#### A. Distribution function and velocity autocorrelation

In Fig. 2(a) we show the distribution function  $f(c)$  of the rescaled velocity  $c \equiv v/v_0$  [with  $v_0 \equiv (2T/m)^{1/2}$  being the thermal velocity and  $T \equiv (m/2)\langle v^2 \rangle$  the granular temperature, and  $\langle \dots \rangle$  denotes ensemble average]. Except when specified otherwise, magnitudes are dimensionless. We use particle diameter  $\sigma$ , seconds  $s$ , and particle mass  $m$  as units for length, time, and mass respectively.

The results show a clear tendency to deviate from the Maxwellian distribution function (represented here by a solid line), this trend being stronger the denser the system. As observed in previous experimental works on quasi-2D granular dynamics, as the tails deviate from the Maxwellian, they become exponential-like [52–54].

Moreover, it is interesting to note that this behavior was previously reported for constant particle density series with increasing granular temperature, but not for (approximately) constant temperature series, as displayed in Fig. 2(a). We chose to compare systems with similar temperature in order to isolate the effects of modifying  $\phi$  from the effects of changing the energy input-dissipation balance. There is a certain difficulty in creating these constant temperature series, since the range of attainable granular temperatures can be very narrow depending on particle density.

Figure 2(b) shows the kurtosis  $K = \langle v^4 \rangle / \langle v^2 \rangle^2$  of the distribution function, which can be used to quantify the deviations from the Maxwellian distribution. As we can see, there is also a strong overall tendency to deviate significantly from the Maxwellian at low temperatures and low densities [see

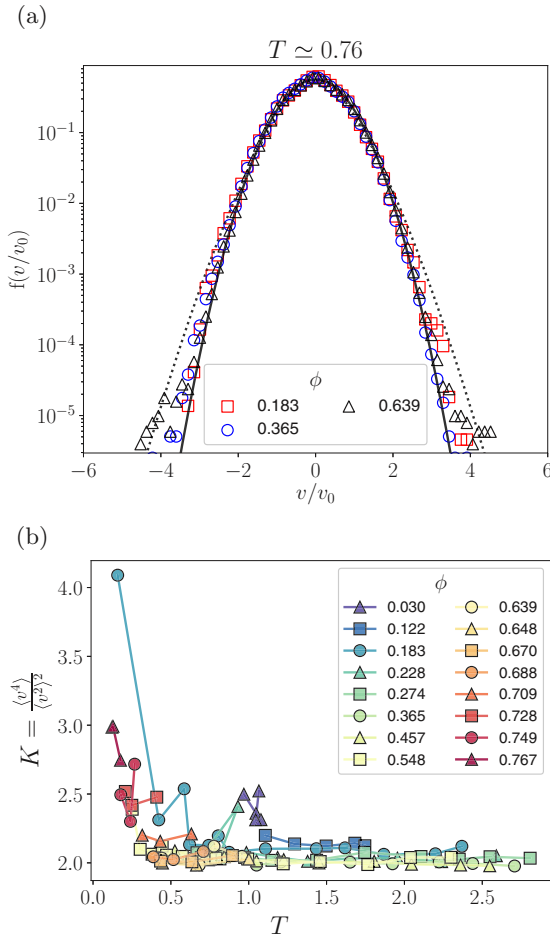


FIG. 2. (a) Velocity distribution functions in logarithmic scale for a series taken at approximately constant granular temperature. The experimental data reveal that high density systems will exhibit more pronounced non-Maxwellian high-energy tails at  $T = 0.76$ . (b) Here we represent the kurtosis for constant density series vs  $T$ .

Fig. 2(b)]. This probably signals the prevalence in this regime of friction effects due to the interaction between the irregular mesh surface and the balls, and, as we will see later, can also be an indication of ordering processes.

The velocity autocorrelation function (VAF) reflects the memory effects in the fluid and is related to key transport properties. Within our experimental accuracy, it has been verified to depend only on time differences. We thus define this quantity as follows:

$$A(t) = \frac{\langle \vec{v}(\tau) \cdot \vec{v}(t + \tau) \rangle}{\langle \vec{v}(\tau) \rangle^2}, \quad (1)$$

where  $\langle \dots \rangle$  indicate averaging over particles  $i$  and time  $t$ , with a time step  $\tau$ .

Results are shown in Fig. 3, where it can be readily noticed that there is a significant time interval during which autocorrelations are negative. We interpret this as a clear indication of particle effects due to noncontact distance interactions mediated by the circulating air, as opposed to the behavior for hard particles [55]. Moreover, the decay time to negative autocorrelations can be regarded as a measure of the typical collision

time (in this context, “collision” should be understood as a particle entering a region where it can feel the repulsive forces as it approaches other neighboring particles). This collision time has been found to decrease with increasing density.

In order to characterize this effect, Fig. 3(d) presents measurements of the velocity autocorrelation for a wide range of densities at nearly constant temperature. The displayed results clearly indicate that noncontact interactions are in general more important at both ends of the density spectrum. At very low densities the negative dip in the time behavior can be due to a single-particle effect (e.g., vortex shedding). At lower densities the negative values extend even up to  $t \sim 2$  s, indicating that the particles are caged by their neighbors. Interestingly, the behavior is not monotonic, and, in the very dense regime, the dip becomes more pronounced again. This indicates that the interstitial hydrodynamic effects are more complex than expected, this having an impact in the phase behavior of the system, as results reveal later. Notice for instance that the curve for  $\phi = 0.365$ , with only negative values at short times, presents behavior analogous to that of a gas, whereas for both lower and higher densities stronger negative autocorrelations at longer times show up, which is the behavior that can be expected for a liquid. However, as diffusive properties will reveal, it is at the lowest density ( $\phi = 0.183$ , purple symbols curve) where we can actually detect the strongest negative autocorrelations, indicating that what we are detecting is actually a glass phase. Finally, at very high densities, negative correlations become stronger than in the liquid, this being precursor evidence of a symmetry break (crystals developing). Thus, velocity autocorrelations seem to suggest the following phase sequence for increasing density: glass, gas, liquid, crystal.

### B. Diffusion

An important characteristic of the experimental particles’ random motion is the mean square displacement (MSD)  $\langle r^2 \rangle$ . Most frequently, systems exhibit a power-law long-time behavior of the MSD, i.e.,  $\langle r^2 \rangle \sim D_\alpha t^\alpha$ , where  $\alpha$  is the diffusion exponent, whereas  $D_\alpha$  is the diffusion coefficient. If  $\alpha \neq 1$ , the diffusion process is anomalous; in particular, it is called subdiffusive when  $\alpha < 1$ .

The drawback of only having at our disposal a limited number of trajectories can be alleviated through the standard procedure [56,57] of constructing the time average of the mean square displacement (TAMSD) for each trajectory,

$$\overline{r^2(t)} = \frac{1}{t_m - t} \int_0^{t_m - t} d\tau |\vec{r}(\tau + t) - \vec{r}(\tau)|^2 \quad (2)$$

( $t_m$  is the measurement time), and subsequently taking the mean over the ensemble of time averages for the individual trajectories. This yields the ensemble average of the time averaged mean square displacement (ETAMSD)  $\langle \overline{r^2(t)} \rangle$ .

In this procedure it is assumed that both the MSD  $\langle r^2 \rangle$  and the TAMSD  $\overline{r^2(t)}$  follow the same power-law dependence  $t^\alpha$ , so that  $\alpha$  can be accurately computed from a limited number of trajectories. However, this is not always the case. A well-known counterexample exhibiting nonequivalence between the TAMSD and the MSD as a result of weak ergodicity breaking is transport generated by the so-called



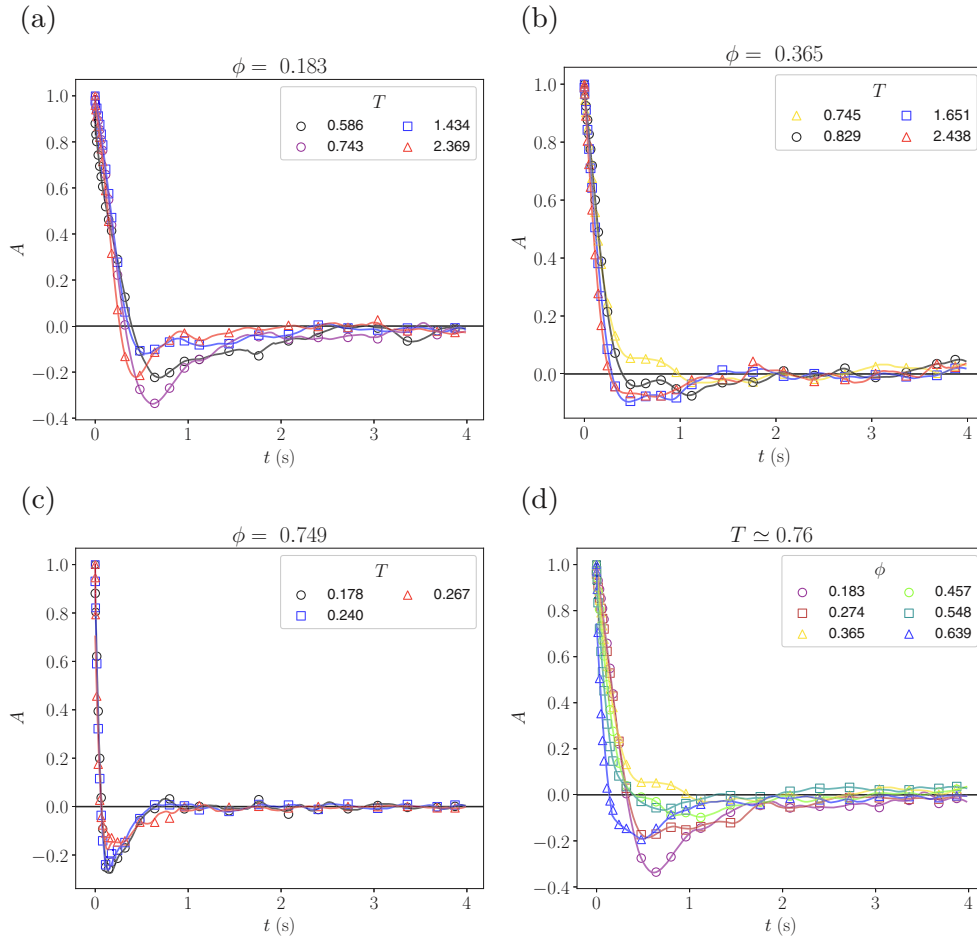


FIG. 3. Velocity autocorrelations. Panels (a), (b), and (c) display data series taken at constant packing fraction ( $\phi = 0.18$ ,  $\phi = 0.365$ , and  $\phi = 0.749$  respectively); (d) shows a data series taken at approximately constant granular temperature.

continuous-time random walk (CTRW) model [56]. Fortunately, in our experimental system, there are no indications of such a behavior (for example, our VAFs are qualitatively different from those obtained from the CTRW model [58]).

In Fig. 4 we show some representative ETAMSD curves obtained from three experiments with  $N = 60$  ( $\phi = 0.183$ ,  $T = 0.422$ ), 120 ( $\phi = 0.365$ ,  $T = 0.618$ ) and 233 balls ( $\phi = 0.709$ ,  $T = 0.632$ ). Only data corresponding to trajectories longer than 40 s are considered. We have carried out fits of the EATMSD in the time interval  $2 < t < 16$  s (gray region in Fig. 4). This choice is a tradeoff ensuring that such an interval starts well after the end time of the ballistic regime, but is at the same time short enough to yield a sufficiently long time window  $t_m - t$ , so that statistical problems in the computation of the time average can be largely avoided.

In a further effort to obtain an improved estimate of  $\alpha$ , we have also plotted curves displaying the time dependence of the so-called mean logarithmic square displacement (MLSD) [57], which is the ensemble average of the logarithm of the TAMSD,  $\overline{\log r^2(t)}$ . A fit of this quantity as a function of  $\log t$  leads, in general, to better estimates for  $\alpha$ , provided that the localization error in the particles position remains small (as is the case in our experiments) [57].

All curves clearly exhibit an initial ballistic regime during which  $\overline{\langle r^2(t) \rangle} \sim t^2$ . This holds up to times  $\lesssim 0.1$  s. The ballistic regime is always followed by a subdiffusive regime ( $\alpha < 1.0$ ). For  $\phi = 0.183$  and  $\phi = 0.365$  one can spot an increase in the slope of the final part of the experimental curves, which could indicate the eventual onset of normal diffusion at even longer times, not covered by our experiment. This terminal increase in the slope has indeed been found to be a typical feature in granular dynamics experiments (e.g., in Ref. [50], both a transient subdiffusive regime and a final normal diffusion regime were identified for a proper parameter choice). Nevertheless, one should bear in mind that the quality of the TAMSD deteriorates for larger values of  $t$ , since for such values the size  $t_m - t$  of the time window over which the average is performed decreases. The offset of the MLSD and ETAMSD lines, quite noticeable for  $\phi = 0.183$ , is not completely unexpected [57]. In this case the fit of the MLSD and ETAMSD curves between  $t = 2$  s and  $t = 16$  s leads to  $\alpha = 0.53$  and  $\alpha = 0.70$ , respectively. However, the case with  $\phi = 0.365$  leads to  $\alpha = 0.8$  and  $\alpha = 0.9$ , respectively, whereas the case with  $\phi = 0.709$  leads to  $\alpha = 0.1$  for the two curves. The noteworthy difference in the values of  $\alpha$  for  $\phi = 0.183$

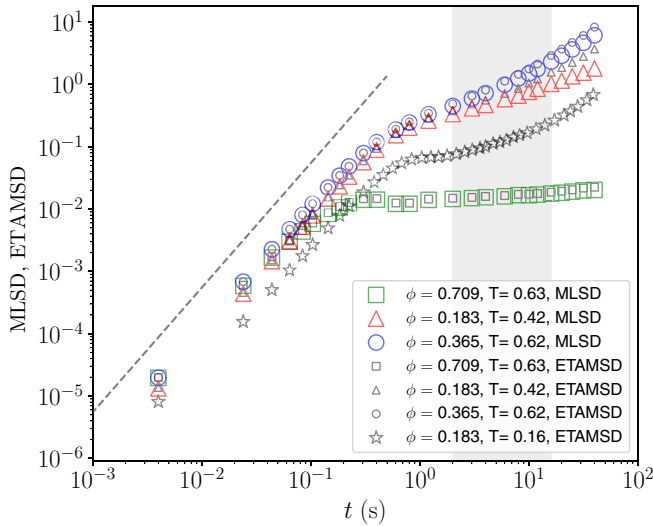


FIG. 4. MLSD (large symbols) and ETAMSD (small symbols) vs time for three experiments with  $\phi = 0.183$  and  $T = 0.422$  (triangles),  $\phi = 0.365$  and  $T = 0.618$  (circles), and  $\phi = 0.709$  and  $T = 0.632$  (squares). The dashed line has a slope equal to 2, characteristic of ballistic behavior. In the diffusive regime (gray region, corresponding to times between  $t = 2$  s and  $t = 16$  s) one has different slopes for different parameter sets. Star symbols correspond to a glassy transition, that typically displays a short plateau forming between ballistic and diffusive regimes.

turns out to be a persistent feature in our experiments; see Fig. 5.

In Fig. 5, we plot the values of  $\alpha$  obtained by using the time interval  $2 < t < 16$  s to fit the MLSD. As a reference, we also provide the values of  $\alpha$  obtained from the ETAMSD computed for a number of experiments. As in Kepten *et al.* [57], we have found that these  $\alpha$  values are generally higher than those yielded by the MLSD (the difference is around 0.1 or, at most, 0.2); yet they follow the same qualitative behavior.

The results in Fig. 5 reveal a large variability of  $\alpha$ , due statistical limitations inherent to our experiments (number of trajectories and limited movie clip duration due to camera memory limitations).

For example, for  $\phi = 0.365$  and  $T = 0.618$ , the MLSD value of  $\alpha$  shown in Fig. 5 is 0.81 (as already mentioned, this value follows from a fit in the interval  $2 < t < 16$  s for trajectories longer than 40 s). However, if one uses trajectories longer than 30 s, one gets  $\alpha = 0.82$ , and if one uses the interval  $1 < t < 20$  s, one finds  $\alpha = 0.80$ . These three different values of  $\alpha$  respectively become equal to 0.90, 0.83, and 0.92 if one chooses  $T = 1.461$ , and for  $T = 1.651$  they are 0.80, 0.89, and 0.77. These cases illustrate the kind of variability in the value of  $\alpha$  that we observe. In any case, if one changes the minimal length of the trajectories and/or the fitting interval in a sensible way, one finds that the corresponding values of  $\alpha$  are compatible with the general qualitative behavior shown in Fig. 5, and in this sense the latter is robust. We note two main regimes, according to the behavior with respect to granular temperature, separated by a small region around  $T = 0.7$  (where the values of  $\alpha$  are close to 1, the normal diffusion exponent). At low temperatures ( $T \lesssim 0.7$ ),  $\alpha$

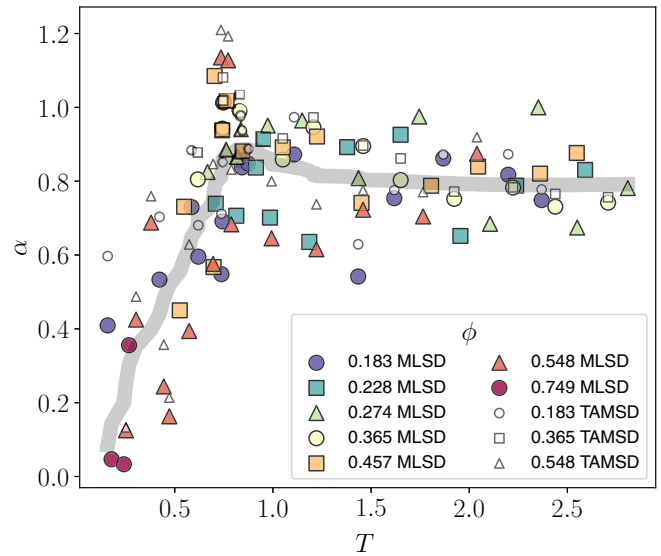


FIG. 5. Diffusion exponent  $\alpha$  vs temperature for several densities. As in Fig. 4, the values of  $\alpha$  were obtained by fitting the ETAMSD and MLSD curves between  $t = 2$  s and  $t = 16$  s. To generate such curves, only trajectories with a minimum length of 40 s have been taken into account. The thick solid gray line is a guide describing the general trend (a smoothing of the MLSD data points was carried out with a third-order Savitzky-Golay moving polynomial).

is clearly increasing with  $T$ . We see that  $\alpha$  remains fairly small for the lowest measured granular temperatures. In particular, we see that there are cases with strong subdiffusive behavior with  $\alpha$  values well below  $\alpha = 0.5$ . Interestingly, these are precisely the cases where the velocity distribution function deviates to a greater extent from a Maxwellian form (see Fig. 2). At higher temperatures, we find a second diffusive regime for which  $\alpha$  displays a plateau vs  $T$  (or at least, is not clearly decreasing or increasing) and for which the values are still subdiffusive but noticeably larger ( $\alpha \sim 0.8$ ) than at very low temperatures.

We think that the strong subdiffusive behavior ( $\alpha \leq 0.5$ ) observed for sufficiently low temperatures is likely due to cage effects [59]. In fact, as density increases, one observes the onset of a crystallization process; see Figs. 7(g) and 7(h) in Sec. IV B (crystals are typically colder than granular fluids under the same forcing conditions [60]). According to [59], the cage size is identified as the value of  $\langle r^2 \rangle^{1/2}$  for which its logarithmic derivative  $d \ln (\langle r^2 \rangle^{1/2}) / d(\ln t)$  attains a minimum. It is interesting to note that in those cases where the ballistic behavior changes to strong subdiffusion (small  $\alpha$ ), the cage effect is so strong that the MSD is even seen to decrease during a short crossover regime. This effect can be clearly observed in the curves corresponding to  $\phi = 0.709$ . We ascribe this behavior to the same transient viscoelastic forces that are responsible for the first dip exhibited by the VAF when  $\phi = 0.183$  and  $\phi = 0.709$  [cf. Figs. 3(a) and 3(c)]. In fact, we conjecture that the anomalous subdiffusive behavior found in noncrystalline phases is due to transient viscoelastic forces characteristic of complex interacting systems with correlated components [56].

In contrast, the high temperature diffusive regime should correspond to regions of the phase space where the dynamics is dominated by a fluid phase [11]. In summary, strong indications of a rich phase behavior in this system emerge out of its diffusive properties. We will address this issue in more detail in the next section.

#### IV. STRUCTURAL PROPERTIES

Phase transitions and crystallization processes were analyzed in the 2D system [24,47,48] with disks but, to our knowledge, not in the pseudo-2D system with spheres. Since interactions between spheres are mediated by strong long-ranged hydrodynamic forces, the phase behavior can be expected to differ importantly from that of the system with disks, where long-ranged forces have not been detected.

Thus, we devote this section to structural properties and phase transitions. Motivated by the lack of previous data on phase transitions in this system, we perform here a comprehensive analysis based on the pair correlation function  $g(r)$  and the Voronoi tessellation with the aim of uncovering as thoroughly as possible the phase transition landscape [61]. As we will see,  $g(r)$  already yields clear indications of different ordering transitions in the system. Voronoi tessellation is a graphical representation that partitions space in cells enclosing only one particle, so that all the points inside a given cell are closer to the associated particle than to any other particle in the system [61]. This representation will confirm the expectations arising from the behavior of  $g(r)$ . Moreover, Voronoi tessellation also conveys additional structural information, thereby providing clear evidence for the onset of hexagonal order at high densities [21,47].

##### A. Radial distribution function

Following a standard procedure, we have computed the radial distribution function from our experimental data; taking into account that the system is 2D and has constant particle density  $\phi_0$ , we employ the following formula:

$$g(r) = \sum_{i,j>i}^N \frac{1}{2\phi_0\pi r_{ij}dr} \Pi(r_{ij} - r - dr/2), \quad (3)$$

where  $\Pi(r_{ij} - r - dr/2) \equiv \Theta(r - r_{ij})\Theta(r + dr - r_{ij})$  is the rectangular pulse function [62] ( $\Theta$  being the Heaviside function [63]).

Measurements of the radial distribution function reveal interesting structural changes in the system, as already advanced in the previous sections. Results are displayed in Fig. 6. As we can see, for  $\phi = 0.183$  [panel (a)] there is a liquid-like structure that is highly dependent on temperature. Notice that, in this case, the main peak appears at a distance clearly larger than  $r = \sigma$  (recall  $\sigma$  is the particle diameter). At a higher density [ $\phi = 0.365$ , panel (b)] an analogous liquid-like structure emerges, but in this case it is very robust against temperature variations. At even higher densities [ $\phi = 0.749$ , panel (c)], we can clearly see a series of sharp peaks, denoting positional ordering. These peaks have been observed in previous studies [46], and their positions are related to the reticular parameter in hexagonal packing. For instance, the secondary

peak at  $r \lesssim 2\sigma$  for instance corresponds to particles in two nonconsecutive vertexes in a hexagonal cell, with one vertex in between, while the secondary peak at  $r \gtrsim 2\sigma$  corresponds to particles in a hexagonal cell located at two non-consecutive vertexes and with two intermediate vertexes. This pattern actually repeats around  $r \sim 3\sigma$ , out of neighbor hexagonal cells, thus indicating long-ranged spatial correlations, inherent to a crystal.

Finally, in Fig. 6(d), the behavior of  $g(r)$  for different densities is displayed in a series of curves at nearly constant temperature, where we can clearly see the transition from fluid-like to crystal-like  $g(r)$  curves as the density is increased. It is worth pointing out that sharp secondary peaks already appear at densities as low (as compared to disks [46,47]) as  $\phi \sim 0.6$ , which is an indication of a lattice parameter that is larger than the particle diameter. Furthermore, the first secondary peak develops around  $r = 2\sigma$ , this being a feature that appears in a crystallization process. Note that this behavior is reminiscent of that observed in early subcooled molecular liquids close to the glass transition [64]. The pair correlation function reveals the emergence of some kind of spatial correlations and translational symmetry, but it does not provide information on the geometrical properties of this symmetry. For that purpose, the Voronoi diagrams, complemented with 2D histograms of particle positions, we present in the next subsection are more adequate.

##### B. Phase changes

In order to detect emerging structural changes, we explored large regions of the parameter space (see Supplemental Material [41] for a list of experimental data). Results below clarify that performing an exhaustive set of experiments at different densities (and granular temperatures) was necessary since the phase behavior is very rich and complex, which otherwise would have remained unnoticed. For instance, the series with varying particle density at constant temperature shows a very rich and peculiar phase behavior. In order to visualize the varying degree of symmetry and the qualitative changes in related properties, we use both 2D spatial histograms and Voronoi tessellation diagrams [61]; see Figs. 7 and 8.

As already anticipated in Sec. II, each of the 2D histograms depicted in Fig. 7 visualizes the positions of each particle (represented by white pixels) averaged over the time duration of each movie ( $\sim 100$  s), as usual in previous studies on phase transitions [5,33]. In contrast, Fig. 8 represents Voronoi diagrams [61] of instantaneous states of the same system. Both figures complement each other, i.e., the 2D spatial histograms tell us about the persistence in time of a given geometrical structure, whereas the Voronoi tessellation diagrams inform us about the specific geometry of that structure.

The evidence provided by Figs. 7 and 8 is rather compelling in spite of the fact that the diagrams correspond to very low densities ( $\phi < 0.1$ ), for which the dynamics is primarily driven by individual particles (particle-particle interactions are not frequent, and the dynamics is expected to be very similar to what has been previously reported for analogous single-particle systems [11]). In contrast, it is interesting to note, that for somewhat larger densities  $0.15 \lesssim \phi \lesssim 0.25$ , we observe glass-like states at sufficiently low temperatures.

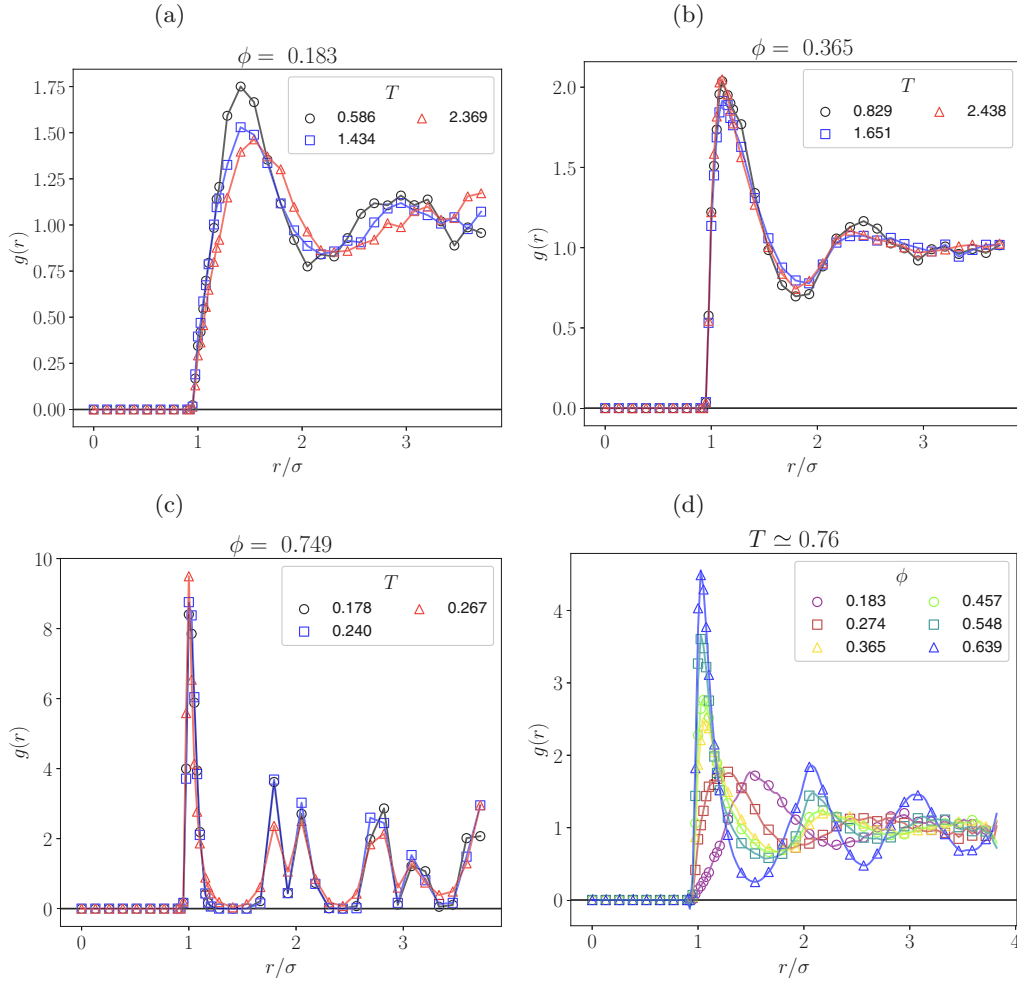


FIG. 6. Pair correlation function as processed from experimental  $xy$  particle positions. Panels (a), (b), and (c) display data series taken at constant packing fraction ( $\phi = 0.18$ ,  $\phi = 0.365$ , and  $\phi = 0.749$  respectively); (d) shows an data series taken at approximately constant granular temperature. A crystallization process is evident from the (a)–(c) panel series; clearly, complete crystallization is attained for  $\phi = 0.749$  [cf. panel (c)].

These glassy phases are characterized by particles staying trapped by their neighbors (cage effect) for a sufficiently long time until they can escape to another cage in which they again remain for a long time, and so on. This is reflected in the diffusive behavior shown in Fig. 4 in the star-symbol series ( $\phi = 0.183$ ,  $T = 0.16$ ), displaying a characteristic plateau (i.e., there is an intermediate region, here at  $t \sim 1$ , for which the curve is horizontal) in the MSD [64]. Indeed, Fig. 7(a) reveals significant inhomogeneities in particle dynamics, with sections of the system (bottom left and top right) where particle positions are more persistent in time; on the other hand, the corresponding Voronoi tessellation [Fig. 8(a)] shows a variety of cells with different coordination numbers, which signals the absence of a clearly dominant symmetry structure. At higher densities ( $0.25 \lesssim \phi \lesssim 0.5$ ), only a single phase is observed, which is seemingly disordered and isotropic, and can therefore be regarded as liquid-like [see panels (c)–(e)]. In panel (f), we have noted an even higher degree of disorder, with particles distributed in a more uniform fashion. Interestingly enough, upon further increase of the density ( $\phi \gtrsim 0.5$ ), we see the development of areas of hexagonal ordering in coexistence

with the fluid phase [see panels (g) and (h)]. The hexagonally ordered phase grows with increasing density, panel (h), eventually occupying the entire system; see panel (i).

It is interesting to note also that hexagonal ordering appears at much lower densities ( $\phi \simeq 0.5$  and higher) than in systems of hard particles [21], in experimental assemblies of disks [46], or in soft disk models used in molecular dynamics to mimic active or passive particles; see, e.g., [65]. We think this signals strong effects of long-ranged hydrodynamic forces between the rolling spheres over the phase behavior. Furthermore, we clearly detected phase coexistence of the hexagonal crystal with the liquid phase [Fig. 7(g)]. This notably differs from the observations of hexagonal crystallization or melting in a confined monolayer of vertically vibrated and quasielastic spheres [21] and in air-fluidized disks [47]. In fact, in these two latter systems the hexagonal crystal undergoes a melting transition of KTHNY [15,17,18,66] type (i.e., the melting transition for the vibrated layer is continuous and mediated by the successive unbinding of dislocation and disclination pairs, and it does not involve phase coexistence). Finally, it is also remarkable that for very cold systems there



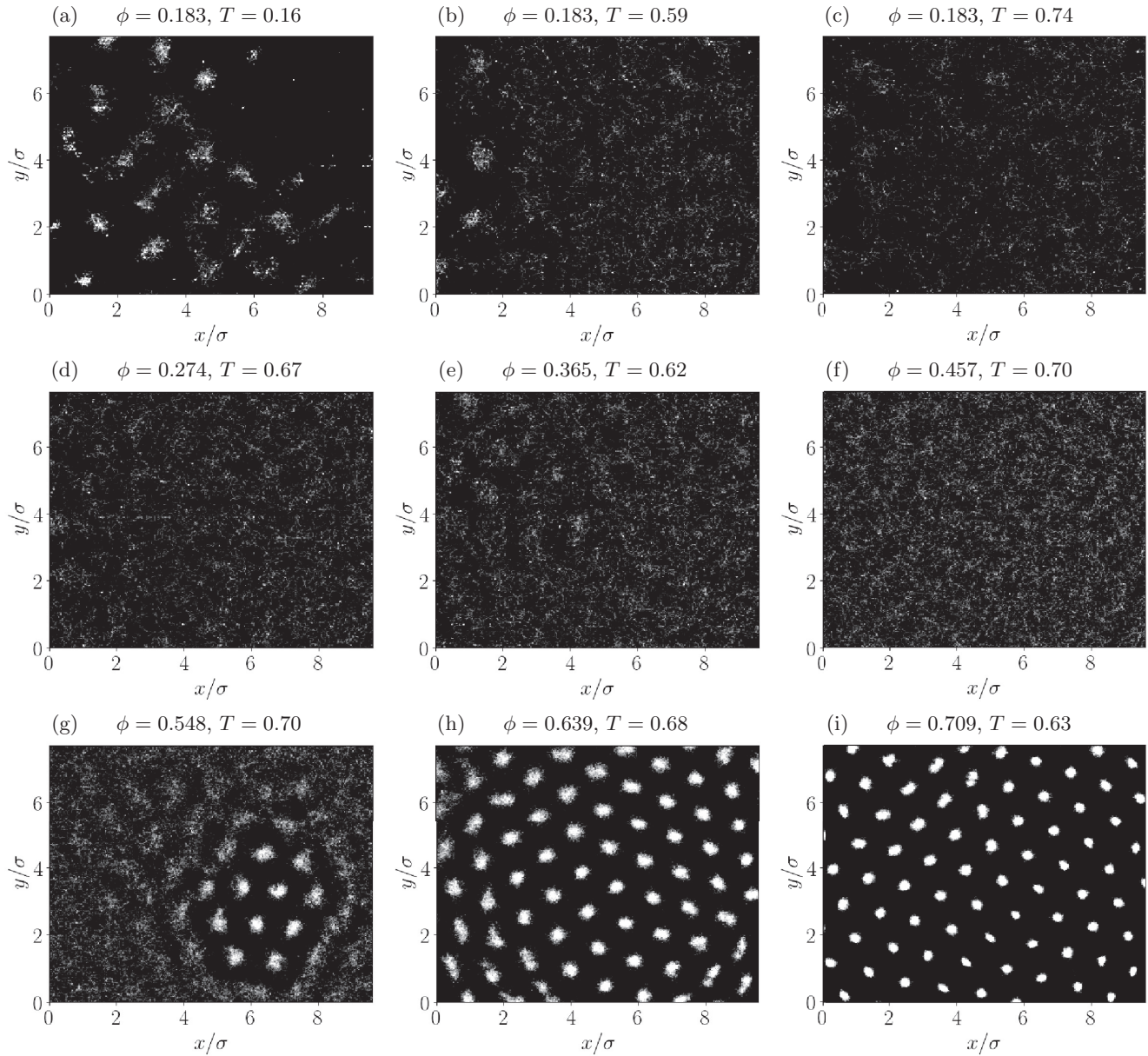


FIG. 7. Set of 2D histograms for different system configurations. These histograms were generated from the complete set of images in the movie clips, each grey dot representing a particle’s instantaneous position. First row: each figure corresponds, from left to right, to increasing granular temperature at constant density; as the system heats up, first glassy behavior and then transition to liquid are observed. Second and third rows: each figure corresponds, from left to right, to increasing density at constant temperature; a transition from liquid to crystal takes place, with phase coexistence.

is no collective ordered collapse, as happens in a vibrated monolayer of hard spheres [5]. Instead, the particles in the gas phase gradually undergo unstructured strong freezing, which results in the collective formation of disordered lattices [Fig. 7(a)].

In addition to Figs. 7 and 8, movie clips and experimental data of the different phases observed are available in the Supplemental Material [41]. The complexity and richness of the phase transitions that we have observed is worth being studied in more detail. Such a study will be carried out in subsequent works.

Finally, in Fig. 9(a) we present in a more quantitative manner geometrical configurations for glass, liquid, and hexagonal crystal, by means of Voronoi histograms (averaged over all frames) according to the particle coordination number (or, equivalently, type of polygon for each Voronoi tile). As we can see, hexagonal cells become predominant only when the hexagonal crystal is fully developed (for  $\phi \geq 0.6$ ), whereas in both glass and liquid the cell distribution is more uniform. In order to quantify the liquid-hexagonal transition more specifically, we represent in Fig. 9(b) the absolute value of the average of the six-bond order parameter  $\Psi_6$  for an

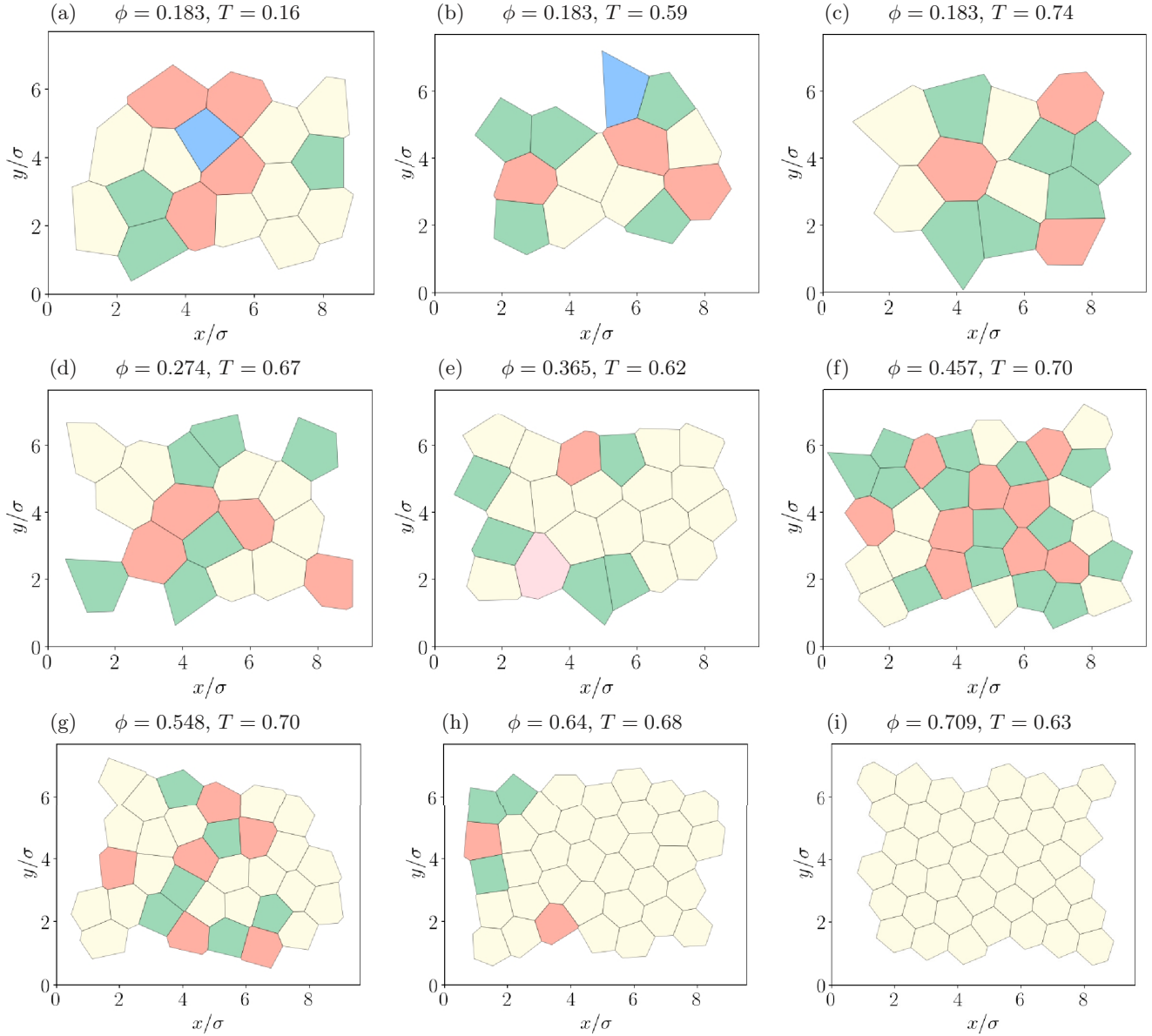


FIG. 8. Voronoi diagrams corresponding to the systems depicted in Fig. 7. These diagrams confirm the glassy behavior in panels (a) and (b), the lack of order in the liquid-like systems, see panels (d), (e), (f), and the emergence (initially in coexistence with a liquid phase) of hexagonal ordering, see panels (g), (h), (i). (Irregular) polygons have been marked according to the following color code: blue for squares, green for pentagons, yellow for hexagons, dark red for heptagons, and light red for octagons.

increasing density series, at constant temperature, and its density distribution functions for three different densities. This order parameter average is defined, for each frame, as  $\Psi_6 = (1/N) \sum_k (1/N_k) \sum_j e^{6\theta_{jk}}$ , where  $\theta_{jk}$  is the bond angle for the  $k$ - $j$  particle pair and the  $j$  sum runs over the  $N_k$  neighbors of particle  $k$  (the sum over the  $k$  particle index is the magnitude averaging, assuming the system has  $N$  particles in total). After this, we average for all frames, which we denote as  $\langle \Psi_6 \rangle$ . A steep increase in  $|\langle \Psi_6 \rangle|$  is noticeable for packing fraction  $\phi > 0.548$ , which is the density corresponding to the system in Fig. 7(g), for which we first find a developing hexagonal crystallite. Also notice here that glass and liquid present rather similar behavior; i.e., cell histograms and six-bond order parameter do not display ordering, which is what we expected

since these phases are indistinguishable by their structural properties.

## V. CONCLUSIONS

We have studied in this work the pseudo-2D dynamics of a set of air-driven identical spheres which, excited by turbulent air, roll under Brownian movement on a horizontal metallic grid.

To the best of our knowledge, we have obtained the first experimental series showing the influence of particle density on the behavior of the distribution function [Fig. 2(d)] at nearly constant temperature. The distribution function exhibits non-Maxwellian high energy tails, a feature also reported in

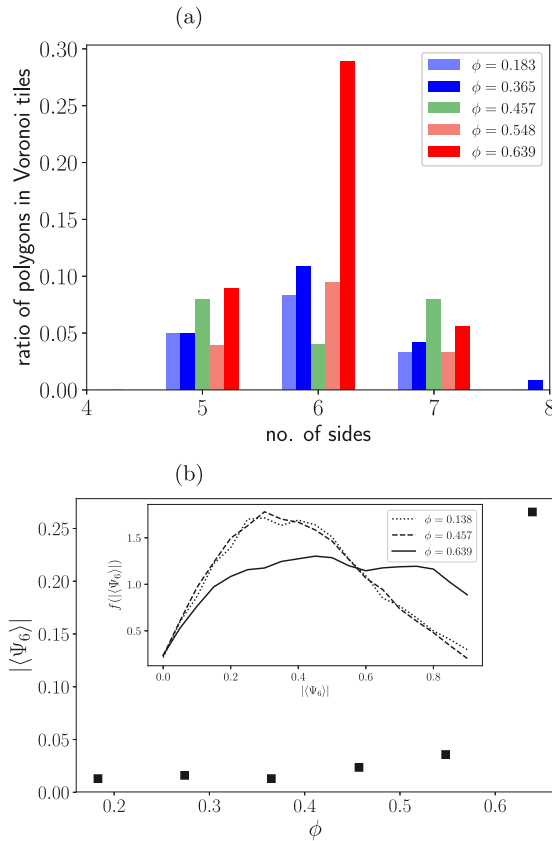


FIG. 9. (a) Voronoi tile histograms, displaying time averaged distributions for different densities. (b) Average of six-bond order parameter,  $|\langle\Psi_6\rangle|$ , for constant temperature series ( $T \simeq 0.76$ ). Its density distribution function is also represented in the inset, for the cases  $\phi = 0.183$  (glass, dotted line),  $\phi = 0.457$  (liquid, dashed line) and  $\phi = 0.639$  (hexagonal crystal, continuous line).

previous works on granular dynamics [5,67]. However, in contrast with the behavior of a monolayer of vertically vibrated particles [53], these non-Maxwellian tails seem to be more prominent at higher temperatures [Figs 2(a)–2(c)].

Velocity autocorrelations illustrate the relevance of hydrodynamic forces due to airflow-mediated particle interactions. Our analysis unveils an important difference with respect to analogous experimental setups, like thin layers of vertically vibrated spheres [21] or air-fluidized disks [47]. In particular, we show that hydrodynamic forces result in the onset large negative autocorrelations at comparatively short times (Fig. 3). Direct observation confirms that particles initially approaching each other then experience an effective repulsion at shorter distances. This yields a very peculiar phase map, as shown in Sec. IV B. In particular, it prevents the formation of gas-like states at very low densities ( $\phi \lesssim 0.15$ ); contrary to the case of air-fluidized disks, we observe independent Brownian-like behavior for each particle, which rarely collides (see Supplemental Material experiment clips [41]). Clearly, the effect of repulsive forces in the dynamics of the system is more important at low densities, which is consistent with the observation that negative autocorrelations at short times are more pronounced in dilute systems [Fig. 3(d)]; see also movies in the Supplemental Material [41]).

Two distinct diffusive regimes have been observed. In contrast with previous works, the system can remain subdiffusive even in disordered low density phases (Fig. 5), which is another consequence of the existence of long-ranged hydrodynamic interactions. We thus see no strong dependence of the diffusion exponent  $\alpha$  on the particle density. In contrast,  $\alpha$  turns out to be very sensitive to changes in the granular temperature. At very low temperatures,  $\alpha$  takes very small values, and the system is strongly subdiffusive. At somewhat higher temperatures, the system still remains strongly subdiffusive despite the steady growth of  $\alpha$  with increasing temperature. Finally, at temperatures  $T \approx 0.7$  and higher,  $\alpha$  stabilizes around values that are weakly subdiffusive and a plateau is observed.

The phase transitions observed in our system display a surprisingly rich and peculiar behavior, not reported previously in similar systems and ranging from a collection of independent Brownian-like particles at low densities to glassy or liquid states at moderate densities, and to the onset of regular hexagonal lattices at higher densities. Most notably, the hexagonal crystal melting occurs here in coexistence with a liquid phase. This finding differs strikingly from previous results reported for 2D systems of air-fluidized disks [47] and quasi-2D systems of quasielastic spheres [21], where phase coexistence of liquid and hexagonal crystals in the melting transition was not found. In our system, the behavior of the liquid to hexagonal crystal transition appears to be more similar to what has been reported for highly inelastic spheres in a quasi-2D system [38], where phase coexistence has also been reported. However, in our system the phase coexistence seems to be mediated by long-ranged hydrodynamic forces rather than by the inelasticity of particle collisions, and thus occurs at noticeably lower densities. Thus, further study on the evolution of the bond-orientational correlation function [68] or the  $p_n$  parameter distribution [69,70] will be needed to cast light on the precise mechanism of this phase transition in future work.

While there is an extensive bibliography referring to engineering applications of air table systems [25], here we have used one such system for a more fundamental purpose, namely, to describe a variety of nonequilibrium quasi-2D phase transitions and to identify the analogies with and departures from equilibrium theories and previous observations in granular dynamics experiments with air-fluidized disks [46,47] and thin vibrated layers [6,38].

Summarizing, our results unveil a very rich and original behavior of our quasi-2D system at various levels (distribution function, diffusion, velocity and spatial correlations, phase transition diagrams, etc.) with respect to its closest analogs. Furthermore, contrary to first observations in quasi-2D granular systems [21], our results suggest that the hexagonal crystal melting transition in granular systems may in general not follow the KTHNY scenario.

#### ACKNOWLEDGMENTS

The authors thank Dr. F. Rietz and Dr. A. Lasanta for fruitful discussions and Prof. J. S. Urbach for valuable discussions and revision of the manuscript. We acknowledge



funding from the Government of Spain through Project No. FIS2016-76359-P and from the regional Extremadura Gov-

ernment through Projects No. GR18079 and No. IB16087, both partially funded by the ERDF.

- [1] M. Faraday, On a peculiar class of acoustical figures; and on certain forms assumed by groups of particles upon vibrating elastic surfaces, *Philos. Trans. R. Soc. London* **121**, 299 (1831).
- [2] L. Bragg and J. F. Nye, A dynamical model of a crystal structure, *Proc. R. Soc. London A* **190**, 474 (1947).
- [3] R. A. Bagnold, Grain structure of sand dunes and its relation to their water content, *Nature (London)* **142**, 403 (1938).
- [4] H. M. Jaeger, S. Nagel, and R. Behringer, The physics of granular materials, *Phys. Today* **49**(4), 32 (1996).
- [5] J. S. Olafsen and J. S. Urbach, Clustering, Order and Collapse in a Driven Granular Monolayer, *Phys. Rev. Lett.* **81**, 4369 (1998).
- [6] P. Melby, F. Vega Reyes, A. Prevost, R. Robertson, P. Kumar, D. A. Egolf, and J. S. Urbach, The dynamics of thin vibrated granular layers, *J. Phys.: Condens. Matter* **17**, S2369 (2005).
- [7] O. Reynolds, On the dilatancy of media composed of rigid particles in contact. with experimental illustrations, *Philos. Mag.* **20**, 432 (1885).
- [8] P. Eshuis, K. van der Weele, D. van der Meer, R. Bos, and D. Lohse, Phase diagram of vertically shaken granular matter, *Phys. Fluids* **19**, 123301 (2007).
- [9] E. Khain and B. Meerson, Onset of thermal convection in a horizontal layer of granular gas, *Phys. Rev. E* **67**, 021306 (2003).
- [10] A. Liu and S. Nagel, Jamming is not just cool anymore, *Nature (London)* **396**, 21 (1998).
- [11] R. P. Ojha, P. A. Lemieux, P. K. Dixon, A. J. Liu, and D. J. Durian, Statistical mechanics of a gas-fluidized particle, *Nature (London)* **427**, 521 (2004).
- [12] P. M. Reis, R. A. Ingale, and M. D. Shattuck, Crystallization of a Quasi-Two-Dimensional Granular Fluid, *Phys. Rev. Lett.* **96**, 258001 (2006).
- [13] G. Castillo, N. Mujica, and R. Soto, Criticality of a Granular Solid-Liquid-Like Phase Transition, *Phys. Rev. Lett.* **109**, 095701 (2012).
- [14] I. Goldhirsch and G. Zanetti, Clustering Instability in Dissipative Gases, *Phys. Rev. Lett.* **70**, 1619 (1993).
- [15] J. M. Kosterlitz and D. J. Thouless, Ordering, metastability and phase transitions in two-dimensional systems, *J. Phys. C* **6**, 1181 (1973).
- [16] Nobel Media, The nobel prize in physics 2016, <https://www.nobelprize.org/prizes/physics/2016/summary/> (2016), prize announcement and press release.
- [17] D. R. Nelson and B. I. Halperin, Dislocation mediated melting in two dimensions, *Phys. Rev. B* **19**, 2457 (1979).
- [18] A. P. Young, Melting and the vector Coulomb gas in two dimensions, *Phys. Rev. B* **19**, 1855 (1979).
- [19] K. J. Strandburg, Two-dimensional melting, *Rev. Mod. Phys.* **60**, 161 (1988).
- [20] J. Friedel, *Dislocations* (Pergamon, New York, 1964).
- [21] J. S. Olafsen and J. S. Urbach, Two-Dimensional Melting far from Equilibrium in a Granular Monolayer, *Phys. Rev. Lett.* **95**, 098002 (2005).
- [22] F. Rietz, C. Radin, H. L. Swinney, and M. Schröter, Nucleation in Sheared Granular Matter, *Phys. Rev. Lett.* **120**, 055701 (2018).
- [23] I. Goldhirsch, Rapid granular flows, *Annu. Rev. Fluid Mech.* **35**, 267 (2003).
- [24] L. Oger, C. Annic, D. Bideau, R. Dai, and S. B. Savage, Diffusion of two-dimensional particles on an air table, *J. Stat. Phys.* **82**, 1047 (1996).
- [25] N. Maw, J. R. Barber, and J. N. Fawcett, The role of elastic tangential compliant in oblique impact, *ASME J. Lubr. Technol.* **103**, 74 (1981).
- [26] L. Kondic, R. R. Hartley, S. G. K. Tennakoon, B. Painter, and R. P. Behringer, Segregation by friction, *Europhys. Lett.* **61**, 742 (2003).
- [27] G. Pontuale, A. Gnoli, F. V. Reyes, and A. Puglisi, Thermal Convection in Granular Gases with Dissipative Lateral Walls, *Phys. Rev. Lett.* **117**, 098006 (2016).
- [28] S. Farhadi, S. Machaca, J. Aird, B. O. Torres Maldonado, S. Davis, P. E. Arratia, and D. J. Durian, Dynamics and thermodynamics of air-driven active spinner, *Soft Matter* **14**, 5588 (2018).
- [29] Y. Grasselli, G. Bossis, and R. Morini, Translational and rotational temperatures of a 2D vibrated granular gas in microgravity, *Eur. Phys. J. E* **38**, 8 (2015).
- [30] G. Gogia and J. C. Burton, Emergent Bistability and Switching in a Nonequilibrium Crystal, *Phys. Rev. Lett.* **119**, 178004 (2017).
- [31] M. X. Lim, A. Souslov, V. Vitelli, and H. M. Jaeger, Cluster formation by acoustic forces and active fluctuations in levitated granular matter, *Nat. Phys.* **15**, 460 (2019).
- [32] D. Pihler-Puzović and T. Mullin, The timescales of granular segregation in horizontally shaken monolayers, *Proc. R. Soc. A* **469**, 20130203 (2013).
- [33] P. Pierański, J. Małecki, W. Kuczyński, and K. Wojciechowski, Melting and the vector Coulomb gas in two dimensions, *Philos. Mag. A* **37**, 107 (1979).
- [34] G. Pérez-Ángel and Y. Nahmad-Molinari, Bouncing, rolling, energy flows, and cluster formation in a two-dimensional vibrated granular gas, *Phys. Rev. E* **84**, 041303 (2011).
- [35] N. Mujica and R. Soto, Dynamics of noncohesive confined granular media, in *Recent Advances in Fluid Dynamics with Environmental Applications*, Environmental Science and Engineering Series (Springer, Berlin, 2016), pp. 445–463.
- [36] T. Schindler and S. C. Kapfer, Nonequilibrium steady states, coexistence, and criticality in driven quasi-two-dimensional granular matter, *Phys. Rev. E* **99**, 022902 (2019).
- [37] G. Castillo, N. Mujica, N. Sepúlveda, J. C. Sobarzo, M. Guzmán, and R. Soto, Hyperuniform states generated by a critical friction field, *Phys. Rev. E* **100**, 032902 (2019).
- [38] Y. Komatsu and H. Tanaka, Roles of Energy Dissipation in a Liquid-Solid Transition of Out-of-Equilibrium Systems, *Phys. Rev. X* **5**, 031025 (2015).
- [39] B. Néel, I. Rondini, A. Turzillo, N. Mujica, and R. Soto, Dynamics of a first-order transition to an absorbing state, *Phys. Rev. E* **89**, 042206 (2014).
- [40] R. P. Ojha, A. R. Abate, and D. J. Durian, Statistical characterization of the forces on spheres in an upflow of air, *Phys. Rev. E* **71**, 016313 (2005).



- [41] See Supplemental Material at <http://link.aps.org/supplemental/10.1103/PhysRevE.103.042903> for information on experimental methods, data, experiments movie clips, and additional figures. Also includes Refs. [45,71–79].
- [42] J. C. Crocker and D. G. Grier, Methods of digital video microscopy for colloidal studies, *J. Colloid Interface Sci.* **179**, 298 (1996).
- [43] J. G. Berryman, Random close packing of hard spheres and disks, *Phys. Rev. A* **27**, 1053 (1983).
- [44] M. Van Dyke, *An Album of Fluid Motion* (Parabolic Press, Stanford, 1982).
- [45] OpenCV, <https://opencv.org/>.
- [46] J. Lemaître, J. P. Troadec, A. Gervois, and D. Bideau, Experimental study of densification of disc assemblies., *Europhys. Lett.* **14**, 77 (1991).
- [47] J. Lemaître, A. Gervois, J. P. Troadec, N. Rivier, M. Ammi, L. Oger, and D. Bideau, Arrangement of cells in Voronoi tessellations of monosize packing of discs, *Philos. Mag. B* **67**, 347 (1993).
- [48] I. Ippolito, C. Annic, J. Lemaître, L. Oger, and D. Bideau, Granular temperature: Experimental analysis, *Phys. Rev. E* **52**, 2072 (1995).
- [49] A. R. Abate and D. J. Durian, Partition of energy for air-fluidized grains, *Phys. Rev. E* **72**, 031305 (2005).
- [50] A. R. Abate and D. J. Durian, Approach to jamming in an air-fluidized granular bed, *Phys. Rev. E* **74**, 031308 (2006).
- [51] A. R. Abate and D. J. Durian, Effective Temperatures and Activated Dynamics for a Two-Dimensional Air-Driven Granular System on Two Approaches to Jamming, *Phys. Rev. Lett.* **101**, 245701 (2008).
- [52] A. Prevost, D. A. Egolf, and J. S. Urbach, Forcing and Velocity Correlations in a Vibrated Granular Monolayer, *Phys. Rev. Lett.* **89**, 084301 (2002).
- [53] J. S. Olafsen and J. S. Urbach, Velocity distributions and density fluctuations in a granular gas, *Phys. Rev. E* **60**, R2468 (1999).
- [54] C. Scholz and T. Pöschel, Velocity Distribution of a Homogeneously Driven Two-Dimensional Granular Gas, *Phys. Rev. Lett.* **118**, 198003 (2017).
- [55] I. K. S. S. R. Williams, G. Bryant, and W. van Meegen, Velocity Autocorrelation Functions of Hard-Sphere Fluids: Long-Time Tails upon Undercooling, *Phys. Rev. Lett.* **96**, 087801 (2006).
- [56] Y. Meroz and I. M. Sokolov, A toolbox for determining subdiffusive mechanisms, *Phys. Rep.* **573**, 1 (2015).
- [57] E. Kepten, I. Bronshteyn, and Y. Garini, Improved estimation of anomalous diffusion exponents in single-particle tracking experiments, *Phys. Rev. E* **87**, 052713 (2013).
- [58] S. Burov, J.-H. Jeon, R. Metzler, and E. Barkai, Single particle tracking in systems showing anomalous diffusion: the role of weak ergodicity breaking, *Phys. Chem. Chem. Phys.* **13**, 1800 (2011).
- [59] F. W. Starr, J. F. Douglas, and S. Sastry, The relationship of dynamical heterogeneity to the Adam-Gibbs and random first-order transition theories of glass formation, *J. Chem. Phys.* **138**, 12A541 (2013).
- [60] A. Lobkovsky, F. Vega Reyes, and J. Urbach, The effects of forcing and dissipation on phase transitions in thin granular layers, *Eur. Phys. J.: Spec. Top.* **179**, 113 (2009).
- [61] W. H. Press, S. A. Teukolsky, W. T. Vetterling, and B. P. Flannery, *Numerical Recipes: The Art of Scientific Computing*, 3rd ed. (Cambridge University Press, Cambridge, UK, 2007).
- [62] W. Ruyé, *Introduction to Orthogonal Transforms: With Applications in Data Processing and Analysis* (Cambridge University Press, Cambridge, UK, 2012).
- [63] NIST Digital Library of Mathematical Functions <https://dlmf.nist.gov/>.
- [64] A. Rodríguez-Rivas, J. M. Romero-Enrique, and L. F. Rull, Molecular simulation study of the glass transition in a soft primitive model for ionic liquids, *Mol. Phys.* **117**, 3941 (2019).
- [65] P. Digregorio, D. Levis, L. F. Cugliandolo, G. Gonnella, and I. Pagonabarraga, Clustering of topological defects in two-dimensional melting of active and passive disks, [arXiv:1911.06366](https://arxiv.org/abs/1911.06366).
- [66] B. I. Halperin and D. R. Nelson, Theory of Two-Dimensional Melting, *Phys. Rev. Lett.* **41**, 121 (1978).
- [67] T. P. C. van Noije and M. H. Ernst, Velocity distributions in homogeneous granular fluids: the free and the heated case, *Granul. Matt.* **1**, 57 (1998).
- [68] A. Pasupalak, L. Yan-Wei, R. Ni, and M. Pica Ciamarra, Hexatic phase in a model of active biological tissues, *Soft Matter* **16**, 3914 (2020).
- [69] A. Rodríguez-Rivas, J. M. Romero-Enrique, L. Full, and A. Milchev, Observation of a tricritical wedge filling transition in the 3D Ising model, *Europhys. Lett.* **108**, 26003 (2014).
- [70] A. Milchev, M. Müller, K. Binder, and D. P. Landau, Interface Localization-Delocalization in a Double Wedge: A New Universality Class with Strong Fluctuations and Anisotropic Scaling, *Phys. Rev. Lett.* **90**, 136101 (2003).
- [71] S. Taneda, Visual observations of the flow past a sphere at reynolds numbers between  $10^4$  and  $10^6$ , *J. Fluid Mech.* **85**, 187 (1978).
- [72] AMETEK, Phantom high speed camera.
- [73] F. V. Reyes, A. Santos, and G. M. Kremer, Role of roughness on the hydrodynamic homogeneous base state of inelastic spheres, *Phys. Rev. E* **89**, 020202(R) (2014).
- [74] D. Allan *et al.*, Python code soft-matter/trackpy: Trackpy v0.4.2 (2019), <https://github.com/soft-matter/trackpy>.
- [75] Y. Lanoiselée, G. Briand, O. Dauchot, and D. S. Grebenkov, Statistical analysis of random trajectories of vibrated disks: Towards a macroscopic realization of Brownian motion, *Phys. Rev. E* **98**, 062112 (2018).
- [76] T. Savin and P. S. Doyle, Static and dynamic errors in particle tracking microrheology, *Biophys. J.* **88**, 623 (2005).
- [77] A. J. Berglund, Statistics of camera-based single-particle tracking, *Phys. Rev. E* **82**, 011917 (2010).
- [78] R. J. Ober, S. Ram, and E. S. Ward, Localization accuracy in single-molecule microscopy, *Biophys. J.* **86**, 1185 (2004).
- [79] R. E. Thompson, D. R. Larson, and W. W. Webb, Precise nanometer localization analysis for individual fluorescent probes, *Biophys. J.* **82**, 2775 (2002).